*Conference on Modelling Fluid Flow (CMFF'09)*
*The 14th International Conference on Fluid Flow Technologies*
*Budapest, Hungary, September 9-12, 2009*

# COMPUTATIONAL HEMODYNAMICS IN MOVING GEOMETRIES WITHOUT SOLVING THE FLUID-STRUCTURE INTERACTION PROBLEM

Franck NICOUD[1], Ramiro MORENO[2], Bruno TAYLLAMIN[3], Ming CHAU[4], Hervé ROUSSEAU[2]

[1] Corresponding Author. Institut de Mathématiques et Modélisation de Montpellier, UMR CNRS 5149, CC51, Université Montpellier 2, 34095 Montpellier Cedex 5,France. Tel.: +33 4 67 14 48 46, E-mail: franck.nicoud@univ-montp2.fr
[2] INSERM U 858 I2MR, University Hospital Toulouse-Rangueil, France. E-mail: moreno.r@chu-toulouse.fr
[3] Institut de Mathématiques et Modélisation de Montpellier, Université Montpellier 2. E-mail: bruno.tayllamin@math.univ-montp2.fr
[4] Advanced Solutions Accelerator, Montpellier, France. E-mail: mchau@advancedsolutionsaccelerator.com

## ABSTRACT

Morphological (MRI) and hemodynamic (phase contrast MRI) medical data are used to perform functional imaging for arteries. The relevant data (velocity field, wall shear stress, pressure gradient, ...) are the output of the computation of the blood flow that is coherent with the input medical data. The methodology used to avoid solving the complex fluid-structure interaction problem while accounting for the wall motions is presented first. Results corresponding to phantoms of an abdominal aortic aneurysm and of an aortic cross are then presented to establish the capabilities of the method to account for the Windkessel effect. The potential of the approach is then illustrated by displaying results from the computation of an actual pathological aortic cross.

**Keywords: Aneurysm, Arteries, Computational Fluid Dynamics, Functional imaging, Magnetic Resonance Imaging, Wall motion**

## NOMENCLATURE

| | | |
|---|---|---|
| $\Omega$ | [-] | Volume of the image |
| $\alpha$ | [-] | Weight coefficient |
| $F,F_1,F_2$ | [-] | Cost functions |
| $I$ | [-] | Pixel value |
| $\|J\|$ | [-] | Jacobian of the transformation $T$ |
| $\underline{x}$ | [$m$] | Position in the image |
| $T$ | [-] | Mapping between images |

**Subscripts**

| | |
|---|---|
| target | image to obtain after application of $T$ |
| native | image to which $T$ is applied |

## 1. INTRODUCTION

Risk factors for cardiovascular disease (hypertension and high cholesterol) and their role have been identified, but cannot explain the observed localized occurrence and the progression of the disease (stenosis, aneurysm rupture, aortic dissection). Currently, available techniques such as Computed Tomography (CT), Magnetic Resonance Imaging (MRI) and Ultrasound (US) do not allow accurate determination of the complex velocity distribution and biomechanical load on the arterial wall. Nevertheless there is no doubt that medical imaging is an essential tool for the understanding of these pathological processes. Cardiovascular disease are clearly multi-factorial and it has been shown that deviations of the normal velocity field (e.g. : changes in wall shear stress) play a key role [1]. Despite many hemodynamic studies carried out with models of arterial bifurcations, especially the carotid artery bifurcation, the precise role played by wall shear stress (WSS) in the development and progression of atherosclerosis remains unclear. Still, it is certain that the mechanical load induced by the fluid on atherosclerotic plaques and their surrounding tissues is of the utmost importance for predicting future rupture (culprit plaques) and preventing ischemic events [2]. In the same way, the risk of rupture of an aortic abdominal aneurysm (AAA) depends more on biomechanical factors than simply on the aneurysm diameter. Although clinical decisions are based only on the latter today, wall tension is a significant predictor factor of pending rupture [3]. Computational Fluid Dynamics (CFD) techniques can provide extremely detailed analysis of the flow field and wall stress to very high accuracy. New advances in simulation techniques could make a significant contribution to a better quantitative knowledge of the biomechanical condition of the arteries and lead to a new understanding via deepened insights into these conditions. Advanced simulations could potentially be used for predicting plaque and aneurysm rupture, improving endovascular prosthesis design, as well as for guiding treatment decisions by predicting the outcome of interventional gesture (i.e. stent coil

technique). However, applying computational fluid dynamics (CFD) to actual pathological regions of the arterial tree is very challenging and has never been done so far with sufficient accuracy and time efficiency to be useful in the clinical practice. Several reasons can be put forward to explain this:

1. the blood rheology is complex and, once coupled to flow motion equations, leads to a set of strongly coupled, highly non-linear set of partial differential equations which is far less understood than the classical Navier-Stokes system,
2. the fluid-structure problem is very stiff because the blood to arterial tissue density ratio is close to unity; from an algorithmic point of view, this means that the fluid and structure equations must be advanced simultaneously in time, leading to potentially costly methods,
3. the arterial wall rheology is essentially unknown and hardly measurable because pathology and patient specific ; uniform linear elasticity is most often assumed as a first step, but no reliable data are available to produce the second step,
4. the external load to which the artery is submitted to is unknown,
5. pointwise hemodynamic data with sufficient time and space resolution are hardly measurable under in vivo conditions, although they are necessary to feed the CFD simulations with realistic boundary conditions,
6. accurate geometrical data about the arterial region require advanced medical imaging systems that are only available in radiology department of hospitals whose first objective is to host and treat patients and where neither the computing science nor the computational mechanics are part of the common expertise and background.

To overcome most of the above mentioned difficulties, we propose a new methodology where advanced medical imaging techniques and CFD methods are inter-connected in order to obtain biomechanical data related to the blood flow under realistic and physiological conditions. This leads to a numerical chain whose input come from an entirely non-invasive 4D MRI protocol that provides time varying geometry and flow rates and output is a functional imaging description of the arterial tree region of interest. The paper is organized as follows: the methodology is presented in section 2 where the generation of the 4D meshes is briefly discussed. The results obtained for two phantoms are then presented in section 3, including an abdominal aortic aneurysm (AAA) and an aortic cross (AC). Results from an actual pathological AC after stenting are displayed shortly in section 4.

## 2. METHODOLOGY

The methodology developed relies heavily on advanced medical imaging techniques and dedicated numerical tools for solving the fluid flow equations. It aims at producing functional imaging for arteries by determining the blood flow which is coherent with the geometry deformation and the inlet/outlet hemodynamic conditions that can be obtained from MRI protocols. This is sketched in figure 1 where the square boxes correspond to the tools involved and the generated data are inside ellipses. Some details about the different tools involved are given in the following subsections.

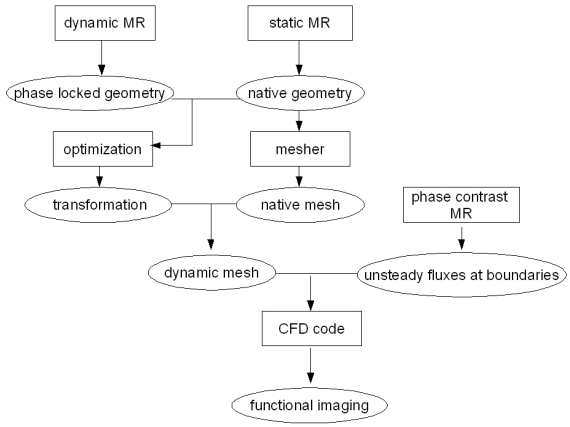


**Figure 1. General methodology to produce functional imaging in arteries**

### *2.1. Geometry acquisition*

A routine contrast-enhanced MR angiography (CE-MRA) was performed using a three-dimensional (3D) slab covering the whole phantom geometry, with an injection of 18 ml of gadolinium diethylenetriamine pentaacetic acid (Gd-DTPA) and with a spatial resolution close to 1x1x1 mm (isotropic voxel). The CE-MRA sequence used phase reordering and data were acquired using parallel imaging so that this acquisition collects the image contrast very fast and become 'phase locked'. This leads to a spatially well resolved description of the vessel geometry at one single phase over the cycle. A single apnea (13s) is necessary for this first acquisition step. Classical segmentation techniques like the level-set [4] can then be applied to this image volume in order to generate the corresponding wall surface. We then make use of a commercial CFD mesh generator (e.g. [5]) in order to reconstruct the full arterial morphology through a triangular surface mesh discretization. Finally, a three-dimensional volume grid based on tetrahedra is generated. The latter is classically used to perform rigid model unsteady fluid simulations and/or coupled fluid-structure computations. Instead, in the present study it serves as a native geometry/mesh which is deformed in

such a way to reproduce the wall motions that can be observed from dynamic geometry acquisition. In this work we used a retrospective triggered True FISP (fast imaging with steady-state precession) imaging, because it has a number of advantages over other techniques (full coverage of the cardiac cycle, intrinsic high signal-to-noise ratio, high signal of blood, short scan time and intrinsic flow compensation). This MRI sequence provides the 3D geometry corresponding to several instants (typically 15-25) over the cycle. The price to pay is a longer acquisition time (a single apnea (25s) is necessary for this second acquisition step) and a coarser spatial resolution (approx. 2x2x2 mm). It is however judged sufficient to gain information about the deformation of the native geometry.

### *2.2. Moving mesh*

Wall motions are imposed to the native mesh consistently with the outcome of the dynamic acquisition [6]. For each phase of the dynamic acquisition, the transformation process consists in estimating the deformation between the native geometry and the geometry corresponding to this particular phase. Therefore, the whole transformation is completed when the deformations to all the target images of a cardiac cycle are computed. At each step, the deformation field results from an optimization problem whose solution is the best compromise between effective and regular transformation. If one seeks for the transformation $T(\mathrm{x})$ which transforms the native image $I_{\mathrm{native}}(\underline{\mathrm{x}})$ into a target image $I_{\mathrm{target}}(\underline{\mathrm{x}})$, the effectiveness of $T$ is measured as

$$F_1 = \int_{\Omega} \left[ I_{native}(\underline{x}) - I_{target}(T(\underline{x})) \right]^2 d\Omega$$

where the integral is taken over the volume of the native image and $I_i$ stands for the pixel values of image i. On the other hand, the regularity of $T$ is assessed as

$$F_2 = \int_{\Omega} \left[ |J(\underline{x})| - 1 \right] d\Omega + \int_{\Omega} \left[ |J(\underline{x})|^{-1} - 1 \right] d\Omega$$

where $|J|$ stands for the Jacobian of $T$ and $F_2$ is designed in order to drive $|J|$ toward unity. The optimization process consists in finding $T$ by minimizing a linear combination of $F_1$ and $F_2$:

$$F = F_1 + \alpha F_2 \qquad (1)$$

where $\alpha$ is a free parameter which should be chosen of order unity. The derivative of $F$ is computed either with symbolic differentiation or by finite differences and a simple steepest descent algorithm is used to minimize Eq. 1.

### *2.3. Hemodynamic data*

In principle, only the knowledge of the inlet unsteady fluxes is required to performed the computations and find out the flow which is consistent with the measured geometrical variations. To this respect, 2D Phase-Contrast (2D-PC) sequences are performed with the MRI system. These sequences are done in planes orthogonal to the vessel axis at the inlets/outlets of the region of interest. In the case of the phantom of the aortic cross, supplementary sagittal 3D-PC acquisition with three velocity encoding directions, covering the whole phantom geometry and the whole cardiac cycle, were performed to compare quantitatively the velocity results from the CFD to the direct measurement. For 2D-PC and 3D-PC, the in-plane spatial resolution and slice thickness were close to 2 mm and 5 mm respectively. A single apnea (15s) is necessary for each 2D-PC acquisition step.

### *2.3. Numerical method*

The flow simulations were performed using the finite volume (FV) method, as implemented in the AVBP code [7, 8] (CERFACS, European Center for Research and Advanced Training in Scientific Computation, Toulouse, France). The FV method used in the code solves the full compressible Navier-Stokes equations that govern the flow. This code makes use of an efficient explicit Arbitrary Lagrangian Eulerian (ALE) formulation which allows imposing the motion of tetrahedral mesh within cardiac cycles. It has been specially designed to reproduce unsteady flows with a minimum amount of artificial viscosity; it relies on advanced numerical schemes [9] and characteristic based boundary conditions [10]. The characteristic Mach number in blood flows is obviously close to zero and for this study it would be more efficient to solve the incompressible Navier-Stokes equations. However, a compressible 3D solver [7, 8] has been used because certain efficient numerical techniques (e.g. artificial compressibility) to solve the incompressible Navier-Stokes equations lead to an hyperbolic problem. As such they share a common mathematical behavior with the compressible equations, allowing the use of characteristic based boundary conditions. This is particularly useful when developing integral boundary conditions [11] which require only the knowledge of the integral of the inlet flux, as opposed to the pointwise flux which is hardly available in biomedical applications. The characteristic framework is also well suited to defined essentially non-reflecting boundary conditions and thus minimizing the amount of numerical reflections and the need of artificial dissipation [12, 13].

## 3. *IN VITRO* VALIDATION

The methodology presented in section 2 relies only on non-invasive medical imaging techniques and thus can be applied to actual patient to obtain patient specific functional imaging, as illustrated in previous studies [14, 15] for the aortic cross. In this

section however, the method is applied to in vitro test cases with the aim to produce both qualitative and quantitative validation. Two configurations are considered, namely the phantom of an abdominal aortic aneurysm (AAA) and of a human aortic cross (AC). In both cases, the compliance is typical of actual values. The blood is replaced by a non physiologic Newtonian fluid with high shear viscosity and density relevant to blood, viz. $\mu=4\times10^{-3}$ Pa.s and $\rho=1056$ kg/m$^3$ respectively. Note that the problem is thus simplified since the difficulties related to the complex blood rheology do not need to be accounted for in what follows. A discontinuous pump adapted from a Ventricular Assist Device (Thoratec) is used to feed the phantoms with pulsatile fluid flow near to physiological pressure levels. Hemodynamic conditions (time-dependent functions) from the 2D-PC sequences were synchronized with the wall motion and subsequently used as boundary conditions as appropriate.

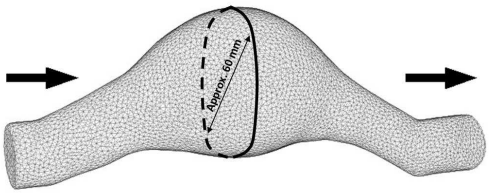


**Figure 2. Computational domain for the phantom of the abdominal aortic aneurysm. The maximum diameter evolves in the range 59-63 mm over the cardiac cycle**

### *3.1. Abdominal Aortic Aneurysm*

The computational domain is depicted in figure 2 where the unstructured mesh is also shown. The flow rate obtained from a 2D-PC sequence is imposed at the inlet (left boundary) while an essentially non-reflecting boundary condition [13] is prescribed at the outlet (right boundary). At the largest cross section area, the aneurysm diameter varies in the range 59-63 mm over the cardiac cycle. Thus its variation due to the wall compliance is approx. 7 %; in many studies, this small relative variation of the diameter is used to justify the rigid wall assumption.

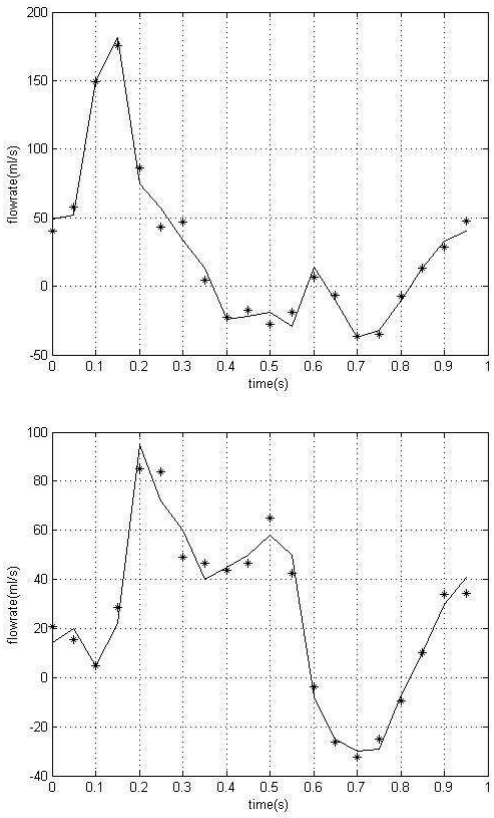


**Figure 3. Time evolution of the flowrate at the inlet (top plot) and outlet (bottom plot) of the AAA. The solid line corresponds to the simulation; the symbols denote the phase contrast MRI measurements**

As shown in Figure 3, the latter is however not justified at all. Indeed, the shape of the outlet flowrate (Fig. 3 bottom) is clearly different from its inlet counterpart (Fig. 3 top). The reason for this difference is that part of the fluid injected into the phantom at systole is stored in the aneurysm since the diameter of the later is the largest when pressure is high (not shown). Later, during the diastole phase, the diameter of the aneurysm recovers its lower value and the fluid that has been stored earlier is released and contributes to the instantaneous flowrate leaving the computational domain through the right boundary. As a result the systolic peak is much wider at the outlet compared to the inlet, as shown in Fig. 3. This figure also indicates that the computation reproduces the so called Windekessel effect very nicely since the CFD and MRI signals are in very good agreement both at the inlet and the outlet. This demonstrates the importance to account for the geometry variations when dealing with cardiovascular flows.

### *3.1. Aortic Cross*

The computational domain is depicted in figure 4 where the position of the cross section displayed in figure 6 is also shown. The flow rate obtained

from 2D-PC sequences are imposed at the ascending aorta (inlet) and at the supra-aortic vessels (outlet). An essentially non-reflecting boundary condition [13] is prescribed at the outlet of the descending aorta.

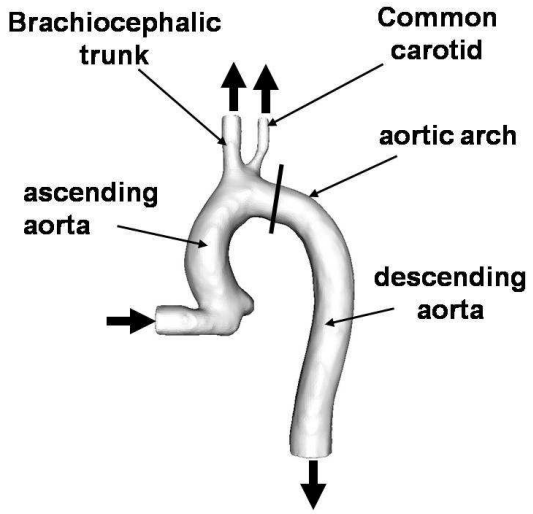


**Figure 4. Computational domain for the phantom of the aorta cross. The bold line shows the position of the cross section displayed in figure 6**

Note that the extra pipe section at the inlet of the computational domain is part of the in vitro model. This one was designed is such a way to promote the swirl motion of the fluid flow at the inlet of the physiological part of the phantom in order to reproduce the in vivo hemodynamic conditions more closely. The simulations began from an initially quiescent flow state and continued for a number of full cardiac cycles in order to allow the development of a fully periodic flow, representative of a regular heartbeat. It was found that the main features of the vascular flow field became periodic within four cycles.

The time evolution of the flowrate is shown in figure 5 for the inlet and outlet sections of the aorta, for both the phase contrast MRI and the computation. As expected, the agreement is better for the inlet where the velocity is imposed as a boundary condition. The difference at the inlet comes from the fact that relaxed boundary conditions are used in order to avoid numerical instabilities [13] by letting most of the high frequency, numerical oscillations leave the computational domain through the boundaries. The price to pay is that physical quantities are not imposed exactly at boundaries ; note however that the difference observed in figure 5 (top) are most probably smaller than the experimental uncertainty related to the PC-MRI based flowrate measurements. Considering the outlet section corresponding to the descending aorta, see figure 5 (bottom), the main features of the experimental signal are well recovered in the numerical results. This supports the idea that the Windkessel effect, related to the storage/release of blood during the cardiac cycle and due to the geometry deformation, is well predicted in this complex geometry.

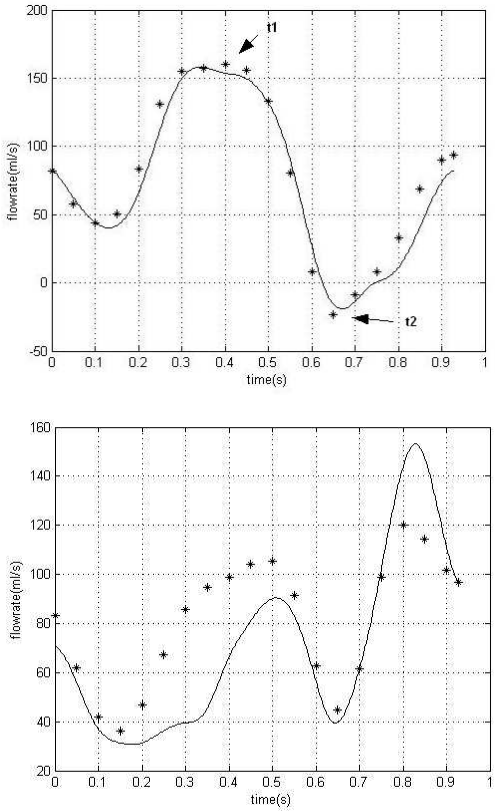


**Figure 5. Time evolution of the flowrate at the inlet (ascending aorta, top plot) and outlet (descending aorta, bottom plot) of the aortic cross. The solid line corresponds to the simulation; the symbols denote the phase contrast MRI measurements.**

Finally figures 6 and 7 offer a comparison of the velocity vectors as obtained from MRI and CFD in the cross section depicted by the bold line in figure 4 and in a sagittal plane respectively. The comparison is made at two instants over the cardiac cycle which are representative of the systole phase (instant $t_1$) and the diastole phase (instant $t_2$) respectively (see figure 5 (top) for the location of $t_1$ and $t_2$). The general agreement is also good, although the spatial resolution is not as good with the phase contrast MRI. The results indicate that the blood flow in the aortic arch is characterized by an intense swirl motion, especially at systole. The strength and the position of this motion are similar in both the experimental and the numerical approaches (see figure 6). Also, the reverse flow which is observed in the experiment at diastole (see

figure 7 (right)) is well recovered in the computation. The general organization of the systolic flow is also comparable in both approaches (see figure 7 (left)), with the jet zone at the outer part of the arch where the speed is the highest and the trend to recirculate below the supra-aortic vessels.

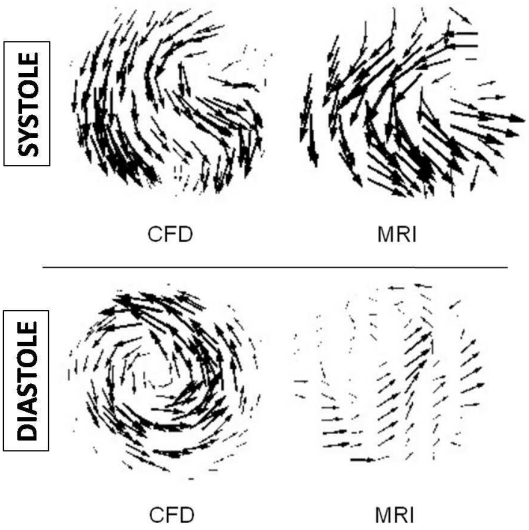


**Figure 6. Velocity vectors obtained from CFD and MRI at systole (top) and diastole (bottom) phase. Plane intersects the upper arch as depicted in Fig. 4**

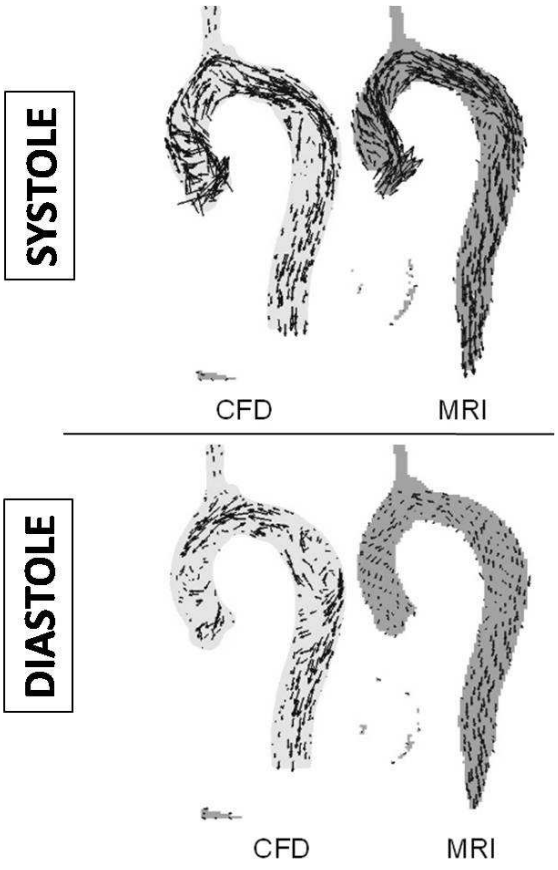


**Figure 7. Velocity vectors obtained from CFD and MRI at systole (left) and diastole (right) phase. Sagittal plane.**

## 4. AN *IN VIVO* APPLICATION

In order to illustrate the potential of the method, it is now applied to the physiological aortic arch of a patient having undergone a severe car crash. This person was treated in emergency at the University Hospital of Toulouse-Rangueil, France. Figure 8 displays an image from a control CT scan performed shortly after an aortic stent has been implemented as a treatment of the injured aorta. The struts of the endo-prosthesis are clearly visible on the image which also reveals the thrombosis generated by the aorta leakage due to the car crash.

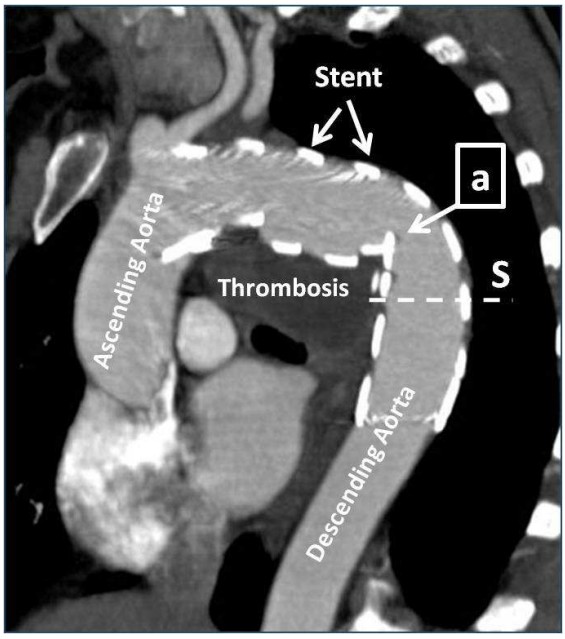


**Figure 8. CT scan performed after stenting. The image displays the ascending and descending aorta as well as the struts of the stent. Label "a" indicates a region with strong cross section area restriction. Section S is a cross section where quantitative velocimetry from PC-MRI is available.**

As depicted in Fig. 8, the implemented stent is long enough to cover the whole aortic arch as well as the beginning of the descending aorta. Due to the geometry of the vessel, it has been fold during its implementation, leading to a restriction in the cross section area (see label 'a' in Fig. 8). This geometrical particularity has a strong impact on the hemodynamics as displayed in Figure 9 which shows an image from an additional phase contrast MRI testing that was performed. In this view, positive vertical velocities are coded in white while negative vertical velocities appear in black. Consistently, the upper region of the arch appears in

grey since the vertical velocity is essentially zero in this region. The enlarged region of interest corresponds to the place where the cross section area is reduced due to the stent folding. It is characterized by a white-black pattern which corresponds to a region where blood particles flow in two opposite directions. From a medical point of view, this situation might induce a waste in mechanical energy and a potential risk for heart fatigue as well as non optimal distal vascularisation. Thus it was used as a test for the methodology presented in this paper.

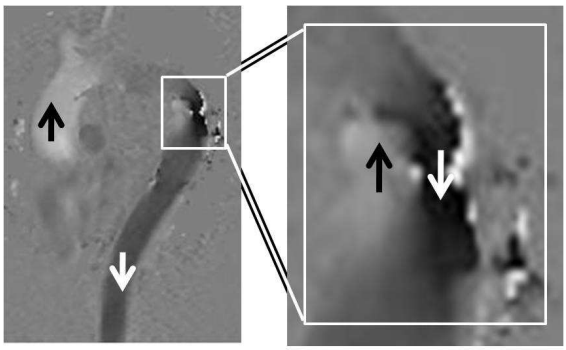

**Figure 9. Phase contrast MRI coding the vertical velocity. Positive values are in white, negative values in black. The white-black pattern visible in the region where the cross section area is reduced indicates possible recirculation.**

Compared to the simulations presented in sections 3.1 and 3.2, the situation is now more complex because **a-** in vivo hemodynamic measurements are more challenging and thus the inlet boundary conditions are not known as precisely, **b-** the blood rheology for this particular patient is unknown and the Newtonian fluid assumption has been done for simplicity, **c-** the characteristics of the distal systemic cardio-vascular system are unknown. Still it is worth investigating whether the proposed methodology can predict the major features of the blood flow. To this respect, Figure 10 displays the computed vertical velocity in a sagittal plane. The positive-negative vertical velocity pattern observed in the phase contrast MRI measurement of Fig. 9 is nicely recovered. To complete this qualitative agreement, a more quantitative comparison of the bulk velocity through section S (see Fig. 8) is provided in Figure 11. The experimental value is available at this particular section because it belongs to the 2D plane used to perform PC MRI assessment of the inlet flux at the ascending aorta. In spite of the complexity of the configuration considered, the general agreement between the CFD and MRI signals is fairly good. Notably, both the position and the amplitude of the main (negative) peak are well predicted by the proposed methodology.

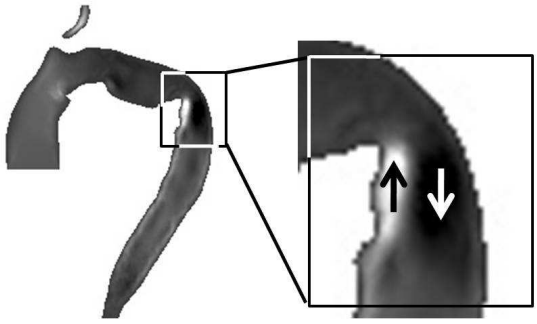

**Figure 10. Computed vertical velocity in a sagittal plane close to the one used in Fig. 9. Positive values are in white, negative values in black.**

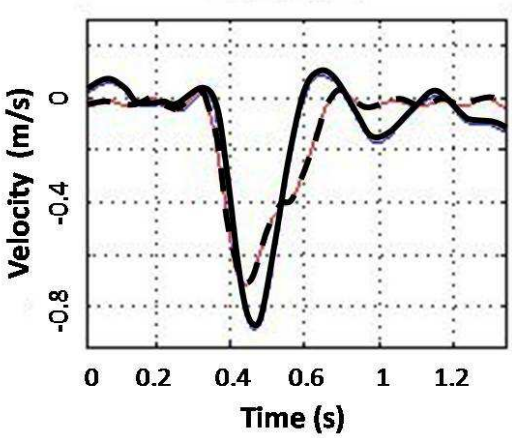


**Figure 11. Time evolution of the bulk velocity through the section S depicted in Fig. 8. Solid line: CFD; dashed line: PC MRI.**

## 5. CONCLUSIONS

A numerical chain is proposed in order to generate functional imaging relevant to arteries. It relies on several imaging techniques (contrast enhanced magnetic angiography, dynamic MRI, 2D phase contrast MRI) in order to gain data about the deformation of the 3D arterial domain of interest as well as associated hemodynamic conditions at inlet/outlet boundaries. An optimization procedure is then used together with classical segmentation and meshing techniques in order to produce a time evolving 3D mesh which reproduces the observed motions. Once synchronized with the wall motions, the hemodynamic data are used as boundary conditions of a CFD tool for the computation of the (unique) unsteady blood flow which is consistent with the acquired data. This methodology was applied to the phantoms of a human abdominal aortic aneurysm and aortic cross respectively. For the latter, additional PC MRI sequences have also been performed in order to provide quantitative data about the 3D blood flow. The comparisons made

are reasonable, given the fact that the experimental protocol used is directly transposable to in vivo cases and that associated uncertainties are quiet large. Still, the impact of the Windkessel effect on the flowrate profiles over the cardiac cycle is well recovered numerically in both the AAA and the AC in vitro configurations. The potential of the proposed methodology for the generation of functional imaging in clinical routine was further assessed by considering an actual pathological aortic arch. Again, the proposed MRI/CFD-based method was able to retrieve the flowrate time evolution at a particular cross section along the arch. More importantly, a strong recirculation pattern visible in a control CT scan performed after stenting of the arch was also recovered from the simulation, demonstrating the potential of the approach in terms of hemodynamic characterization of actual arterial tree regions.

## ACKNOWLEDGEMENTS

This work was conducted in the framework of the OCFIA research program funded by the Agence Nationale de la Recherche (ANR-07-CIS7-006-02). The authors are grateful to CINES (Centre Informatique National de l'enseignement supérieur) for giving access to super-computing facilities.

## REFERENCES

[1] Caro C., Fitz-Gerald J., and Schroter R., 1969, Arterial wall shear and distribution of early atheroma in man. *Nature*, 223, 1159–1160.

[2] Corti R., Badimon L., Fuster V., and Badimon J. J., 2002, Assessing and Modifying the vulnerable atherosclerotic plaque, *Chapter Endothelium, flow, and artherothrombosis.* American Heart Association.

[3] Hall A. J., Busse E. F., McCarville D. J., and Burgess J. J., 2000, Aortic wall tension as a predictive factor for abdominal aortic aneurysm rupture: improving the selection of patients for abdominal aneurysm repair. *An Vasc Surg*, 14(2), 152–157.

[4] Malladi R. and Sethian J. A., 1998, Level set methods for curvature flow, image enhancement, and shape recovery in medical images. In *Proceedings of Conference on Visualization and Mathematics*, Berlin, Germany.

[5] Amira 4.1, TGS, Mercury Computer Systems, USA.

[6] Moreno R., Nicoud F., Veunac L., and Rousseau H., 2006, Non-linear transformation field to build moving meshes for patient specific blood flow simulations. In *Wesseling P., Onate E., and Periaux J., editors, European Conference on Computational Fluid Dynamics*, The Netherlands.

[7] AVBP Code :http ://www.cerfacs.fr/cfd/avbp_ code.php and http ://www.cerfacs.fr/cfd/ CFDPublications.html.

[8] Schönfeld T. and Rudgyard M. A., 1999, Steady and unsteady flows simulations using the hybrid flow solver avbp. *AIAA Journal*, 37(11), 1378–1385.

[9] Colin O. and Rudgyard M., 2000, Development of high-order taylor-galerkin schemes for unsteady calculations. *J. Comput. Phys.*, 162(2), 338–371.

[10] Poinsot T. and Lele S., 1992, Boundary conditions for direct simulations of compressible viscous flows. *J. Comput. Phys.*, 101(1), 104–129.

[11] Nicoud F. and Schönfeld T., 2002, Integral boundary conditions for unsteady biomedical cfd applications. *Int. J. of Num. Meth. in Fluids*, 40, 457–465.

[12] Nicoud F., 1998, Defining wave amplitude in characteristic boundary conditions. *J. Comput. Phys.*, 149(2), 418–422.

[13] Nicoud F. and Poinsot T., 2001, Boundary conditions for compressible unsteady flows. In *Tourrette L. and Halpern L., editors, Absorbing Boundaries and Layers, Domain Decomposition Methods. Applications to Large Scale Computation*. Editions Novascience, New-York.

[14] Moreno R., 2007, Simulations Numériques Vasculaires, Spécifiques et Réalistes. PhD thesis, Université Toulouse III.

[15] Moreno R., Chau M., Jeetoo S., Nicoud F., Viart F., Salvayre A., and Rousseau H., 2008, Optimized computational functional imaging for arteries. In *8th International Meeting on High Performance Computing for Computational Science*, Toulouse, France.